Originally published as:

Shi, H., Tian, H., Pan, N., Reyer, C. P. O., Ciais, P., Chang, J., Forrest, M., Frieler, K., Fu, B., Gädeke, A., Hickler, T., Ito, A., Ostberg, S., Pan, S., Stevanović, M., Yang, J. (2021): Saturation of global terrestrial carbon sink under a high warming scenario. - Global Biogeochemical Cycles, 35, 10, e2020GB006800.

DOI: https://doi.org/10.1029/2020GB006800

Saturation of global terrestrial carbon sink under a high warming scenario

Hao Shi[1], Hanqin Tian[1,*], Naiqing Pan[1], Christopher P O Reyer[2], Philippe Ciais[3], Jinfeng Chang[3], Matthew Forrest[4], Katja Frieler[2], Bojie Fu[5], Anne Gädeke[2], Thomas Hickler[4,6], Akihiko Ito[7,8], Sebastian Ostberg[2], Shufen Pan[1], Miodrag Stevanovic[2], Jia Yang[9]

[1]International Center for Climate and Global Change Research, School of Forestry and Wildlife Sciences, Auburn University, Auburn, AL 36849, United States of America
[2]Potsdam Institute for Climate Impact Research, Member of the Leibniz Association, Telegrafenberg, 14412 Potsdam, Germany
[3]Laboratoire des Sciences du Climate et de l'Environment, IPSL-LSCE, CEA-UVSQ-UPSACLAY, Gif sur Yvette F-91191, France
[4]Senckenberg Biodiversity and Climate Research Centre (BiK-F), Senckenberganlage 25, D-60325 Frankfurt am Main, Germany
[5]State Key Laboratory of Urban and Regional Ecology, Research Center for Eco-Environmental Sciences, Chinese Academy of Sciences, Beijing 100085, China
[6]Department of Physical Geography, Goethe University, Altenhöferallee1, D-60438 Frankfurt am Main, Germany
[7]National Institute for Environmental Studies, Tsukuba 305-8506, Japan
[8]Japan Agency for Marine-Earth Science and Technology, Yokohama 236-0001, Japan
[9]College of Forest Resources, Mississippi State University, Starkville, MS 39762, USA

[*]Corresponding author: H. Tian (tianhan@auburn.edu)

Key points

1) Elevated temperature has negative impacts on terrestrial carbon sink.
2) CO_2 effects on terrestrial carbon sink saturate at high CO_2 concentration.
3) Interannual variability of terrestrial carbon sink is more correlated with temperature under RCP2.6 but precipitation under RCP6.0.

Abstract

The terrestrial carbon sink provides a critical negative feedback to climate warming, yet large uncertainty exists on its long-term dynamics. Here we combined terrestrial biosphere models (TBMs) and climate projections, together with climate-specific land use change, to investigate both the trend and interannual variability (IAV) of the terrestrial carbon sink from 1986 to 2099 under two representative concentration pathways RCP2.6 and RCP6.0. The results reveal a saturation of the terrestrial carbon sink by the end of this century under RCP6.0 due to warming and declined CO_2 effects. Compared to 1986-2005 (0.96±0.44 Pg C yr^{-1}), during 2080-2099 the terrestrial carbon sink would decrease to 0.60±0.71 Pg C yr^{-1} but increase to 3.36±0.77 Pg C yr^{-1}, respectively, under RCP2.6 and RCP6.0. The carbon sink caused by CO_2, land use change and climate change during 2080-2099 is -0.08±0.11 Pg C yr^{-1}, 0.44±0.05 Pg C yr^{-1}, and 0.24±0.70 Pg C yr^{-1} under RCP2.6, and 4.61±0.17 Pg C yr^{-1}, 0.22±0.07 Pg C yr^{-1}, and -1.47±0.72 Pg C yr^{-1} under RCP6.0. In addition, the carbon sink IAV shows stronger variance under RCP6.0 than RCP2.6. Under RCP2.6, temperature shows higher correlation with the carbon sink IAV than precipitation in most time, which however is the opposite under RCP6.0. These results suggest that the role of terrestrial carbon sink in curbing climate warming would be weakened in a no-mitigation world in future, and active mitigation efforts are required as assumed under RCP2.6.

Key words: Terrestrial carbon sink, terrestrial biosphere model, interannual variability, global warming, CO_2 fertilization effects

1 Introduction

Terrestrial ecosystems have been serving as the largest natural carbon sink, particularly since the 1960s, sequestering over one fourth of anthropogenic emissions on average [*Friedlingstein et al.*, 2019]. Considering its importance in curbing climate warming [*Friend et al.*, 2014; *Schimel et al.*, 2015], accurately estimating this sink is critical for assessing mitigation policies and activities. A variety of tools, such as eddy covariance observation networks, atmospheric inversions, and terrestrial biosphere models (TBMs), have been developed to improve our understanding of the spatial and temporal patterns of the terrestrial carbon sink and the associated underlying mechanisms. Although significant advances have been achieved, for example in providing an annual updated global carbon budget [e.g., *Friedlingstein et al.*, 2019; *Le Quéré et al.*, 2018], the terrestrial carbon sink remains highly uncertain in terms of the responses of its trend and interannual variability (IAV) to atmospheric CO_2 increase, climate variability and other environmental factors [*Bastos et al.*, 2020; *Green et al.*, 2019; *O'Sullivan et al.*, 2019; *Piao et al.*, 2020; *Trugman et al.*, 2018]. These uncertainties are major caveats for our capability to project carbon-climate feedbacks and their potential influences on human-natural systems [*Huntzinger et al.*, 2017].

The strength of the terrestrial carbon sink has been growing over recent decades [*Ballantyne et al.*, 2012; *Sitch et al.*, 2015]. The increase in atmospheric CO_2 is widely believed to be a dominant factor [*Schimel et al.*, 2015], notably in the tropics [*Sitch et al.*, 2015]. The fertilization effect of elevated CO_2 has been observed in CO_2 enrichment experiments at ecosystem scale [*Norby and Zak*, 2011; *Terrer et al.*, 2019] , inferred from satellite greenness observations [*Donohue et al.*, 2013; *K W Smith et al.*, 2016] and simulated by TBMs as an essential process to account for the carbon sink, but with large differences between models [*Fleischer et al.*, 2019; *Huntzinger et al.*, 2017; *Ito et al.*, 2020; *Kondo et al.*, 2020; *Tian et al.*, 2011b]. However, many studies also raise questions about whether the effect of increasing CO_2 on net land carbon flux is universal and whether it will continue in the future [*Fleischer et al.*, 2019; *Girardin et al.*, 2016; *Hickler et al.*, 2015]. For example, current models do not fully capture the responses observed in field experiments [*Medlyn et al.*, 2015], and no significant positive signal was observed in a four-year ecosystem-scale Free-Air CO_2 Enrichment (FACE) experiment in a mature tropical forest [*Jiang et al.*, 2020]. *Brienen et al.* [2015] also reported that rates of increase in above-ground biomass in Amazon forests have declined by at least one third, potentially due to greater mortality induced by climate variability. Recent studies [*Tagesson et al.*, 2020; *Wigneron et al.*, 2020] confirmed that tropical forests are changing from a carbon sink to carbon neutral or even a carbon source, partly due to droughts, the influences of which on the long-term carbon sink [*Qie et al.*, 2017; *van der Molen et al.*, 2011] and its seasonal cycle [*K Wang et al.*, 2020] have received substantial attention.

The IAV of the terrestrial carbon sink is generally thought to dominate the atmospheric CO_2 growth rate and help constrain our understanding of the strength of carbon-climate feedbacks [*Anderegg et al.*, 2015; *Keeling et al.*, 1995]. The sensitivity of IAV of the tropical land carbon sink to tropical land surface temperature has been taken as an emergent constraint for climate projections by Earth System Models [*Cox et al.*, 2013]. Indeed, *Green et al.* [2019] has demonstrated that land carbon uptake reduction resulting from IAV of water availability even surpasses that induced by the decreasing trend of water availability, causing a positive climate feedback. Although there is a consensus that the IAV of the terrestrial carbon sink is primarily associated with climatic variations, debates exist in terms of the region, biome or climatic factor from which the IAV is sourced [*Ahlstrom et al.*, 2015; *Anderegg et al.*, 2015; *Piao et al.*, 2020; *Poulter et al.*, 2013; *Tian et al.*, 1998]. Semi-arid/arid ecosystems [*Ahlstrom et al.*, 2015; *Poulter et al.*, 2013] and tropical forests [*Anderegg et al.*, 2015; *J Wang et al.*, 2016] have been reported to be a major source of IAV of the global carbon cycle or atmospheric CO_2 growth rate , particularly the latter, whereby tropical mean temperature, tropical nighttime temperature or tropical precipitation have been found to be the determining drivers [*Anderegg et al.*, 2015; *W Wang et al.*, 2013; *Welch et al.*, 2010].

The trend and IAV of the terrestrial carbon sink are also influenced by other factors, such as land use change (LUC) and nitrogen deposition. LUC is the second largest source of greenhouse gas emissions, mainly from tropical deforestation. From 1850 to current times, LUC emissions may contribute approximately one third of the total cumulative anthropogenic emissions [*Houghton and Nassikas*, 2017; *Le Quéré et al.*, 2018]. However, more uncertainty related to LUC-caused carbon emissions has been found than for other components of terrestrial carbon sink. *Houghton* [2010] reported that inventory- or satellite-based estimates of carbon emissions from global land use change could be from 0.9 Pg C yr^{-1} to 2.2 Pg C yr^{-1} in the period 1990-1999.

Nitrogen deposition was estimated to contribute 14% to current terrestrial carbon sink while its synergistic effect with CO_2 contributed another 14% from 1901 to 2016 [*O'Sullivan et al.*, 2019]. But debates exist to the extent to which nitrogen deposition can enhance terrestrial carbon sequestration as minor [e.g., *Nadelhoffer et al.*, 1999] to significant [e.g., *Janssens et al.*, 2010] impacts are reported. Consequently, the estimate of its future long-term impact is highly uncertain [*Reay et al.*, 2008].

These differing results or ambiguities are, in large part, due to limited understanding of biophysical and biogeochemical processes. Such a knowledge gap makes it difficult to be confident in a single TBM in extrapolating local observations to regional and global scales and limits their use as a decision-support tool for mitigation and adaptation measures. To effectively investigate the terrestrial biosphere potential to sequester carbon and the underpinning mechanisms, we adopt an ensemble of TBMs to assess the contemporary and future terrestrial carbon cycle under two contrasted CO_2 trajectories. Specifically, biome sector output data of five TBMs from the Inter-Sectoral Impact Model Intercomparison Project (ISIMIP) phase 2b [*Frieler et al.*, 2017] were used. Different from the Earth System Models (e.g., CMIP5), under each CO_2 trajectory, ISIMIP2b TBMs were run forced by different climate projections that have been bias-corrected to account for climate projection related uncertainties of the carbon cycle. Moreover, the land use dynamics for ISIMIP2b simulations consider impacts of both climate change and socio-economic conditions in future, for example, the irrigation changes [*Frieler et al.*, 2017]. The two contrasting CO_2 trajectories are the Representative Concentration Pathway (RCP) 2.6 and RCP6.0. RCP2.6 is the mitigation scenario very close to the aspirational goal of 1.5 °C warming of the Paris Agreement, while RCP6.0 is a non-mitigation, baseline scenario in which global warming reaches about 3.0 °C [*Frieler et al.*, 2017]. Since ISIMIP2b follows the Shared Socioeconomic Pathway 2 "middle of the road" in future, the high-end no-mitigation RCP8.5 scenario of rough mitigation challenges was not used. This study has two major aims. The first is to project the strength and uncertainty in terrestrial carbon sink over the period 2006-2099 under a mitigation-oriented scenario and a non-mitigation-oriented scenario, closely pertaining to climate policy and mitigations. The second is to determine which factors or processes dominate the modelled trends and IAV in terrestrial carbon sink. A particular focus is on the interacting effects of climate variability with changes in atmospheric CO_2.

2 Methods

2.1 ISIMIP2b experiments

ISIMIP aims to assess and project multi-sectors impacts of climate change by using a variety of sector-specific or multi-sector 'impact models' within the same simulation framework. ISIMIP2b, building on ISIMIP2a which focused on historical simulations, model evaluation and inter-model comparison, coordinates the provision of historical (1860-2005) and future (2006-2099) simulations under a low-end (RCP2.6) and a moderate warming (RCP6.0) scenario [*Frieler et al.*, 2017]. In RCP2.6, the atmospheric CO_2 concentration increase slows down in the first part of 21st century to reach a peak of 443 ppm in 2050, then decreases down to 421 ppm in 2100, due to strong emission mitigation and land-based carbon removal from the atmosphere (Fig. S1a). In RCP6.0, CO_2 increases continuously to reach 670 ppm by 2100 (Fig. S1a).

ISIMIP2b provided land use change and climate projections consistent with the two RCPs. The land use data (Fig. S2) were generated by the global spatially explicit land use model MAgPIE (Model of Agricultural Production and its Impact on the Environment) that optimizes land use and agricultural production patterns under climate-induced changes in crop productivity, water availability and terrestrial carbon content [*Dietrich et al.*, 2019]. The food cropland area is about 250 Mha lower under RCP2.6 than under RCP6.0 (Fig. S1e), but a considerable fraction of land areas (~750 Mha; Fig. S1f) is to fulfill demand for crops dedicated to bioenergy production under RCP2.6, which results in a larger total cropland area than under RCP6.0 [*Frieler et al.*, 2017]. Climate conditions, including historical and future periods, were supplied based on CMIP5 output of four climate models: GFDL-ESM2M, HadGEM2-ES, IPSL-CM5A-LR and MIROC5. These climate data were further bias-corrected at a daily time-step and a 0.5° spatial resolution using the EWEMBI (E2OBS, WFDEI and ERAI data Merged and Bias-corrected for ISIMIP) dataset [*Frieler et al.*, 2017].

We adopted specific simulation experiments to disentangle the role of climate, CO_2 and land-use forcing (Table 1). The RCP-Control experiments considered only climate change for future with both atmospheric CO_2 concentration and land use fixed in 2005, to characterize terrestrial carbon dynamics under different warming scenarios. The RCP-CO_2 experiment considered both time-varying climate and atmospheric CO_2 concentration but with land use change fixed in 2005, and thus the differences of RCP-CO_2 experiments against the RCP-Control experiments gave CO_2 impacts on carbon dynamics, which could be direct (fertilization) or indirect (interaction effects with climate). The RCP-LUC experiments considered changes of all factors, and the differences of the RCP-LUC experiments and the RCP-CO_2 experiments were used to represent LUC impacts. Five TBMs, namely the 'Dynamic Land Ecosystem Model' [DLEM; *Tian et al.*, 2011a], the 'Lund-Potsdam-Jena model with managed Land' [LPJmL; *Bondeau et al.*, 2007], the 'Lund-Potsdam-Jena General Ecosystem Simulator' [LPJ-GUESS; *B Smith et al.*, 2014], the 'Organizing Carbon and Hydrology in Dynamic Ecosystems' [ORCHIDEE; *Guimberteau et al.*, 2018], and the 'Vegetation Integrative Simulator for Trace gases' [VISIT; *Ito and Inatomi*, 2012], were used, but not all four climate datasets were adopted by each model. Finally, there were 17 ensemble members available for all experiments (three by DLEM, two by ORCHIDEE, four by each of the other three models). The performance of these TBMs has been evaluated in ISIMIP2a and the results suggest all models could well reproduce the interannual variation of terrestrial carbon sink and the model ensemble-mean net carbon flux was consistent with long-term independent estimates [*Chang et al.*, 2017]. These TBMs have considerable differences in representing ecosystem processes and ecosystem composition, such as photosynthesis, respiration, carbon allocation, phenology, disturbances, land management and vegetation dynamics (see details in Table S1). Two models, DLEM and LPJ-GUESS, included nitrogen limitation to plant growth and thus partly or fully considered variations in nitrogen inputs, such as biological nitrogen fixation, nitrogen deposition and fertilizer application. It is noted that classifications of land cover types of these TBMs varied but all had the same cropland distribution provided by ISIMIP2b

(Table S1). Outputs of gross primary production (GPP), ecosystem respiration (Re, the sum of autotrophic and heterotrophic respiration), and net biome production (NBP=GPP-Re-other carbon losses, to represent terrestrial carbon sink hereafter) were aggregated to annual time-scale. The positive values of NBP indicate carbon sink while the negative indicating carbon source.

<Table 1>

2.2 Trend and IAV analysis

The ensemble empirical mode decomposition (EEMD) method was used to extract trends of the time series for annual carbon fluxes or meteorology. This method has been proved to be suitable for nonlinear trend analyses while the signal, such as climate change induced vegetation growth or global carbon sink, is non-stationary [*Pan et al.*, 2018; *Piao et al.*, 2020]. The principle of EEMD is to add white noise to the original signal, then decompose the signal into linear or stationary representations of intrinsic mode functions, then repeat the previous two steps but with different white noise, and then calculate the means of ensemble decompositions as the final result [*T Wang et al.*, 2012]. IAV is finally derived as the difference between the original annual timeseries and the EEMD trends. In the analysis of the drivers for terrestrial carbon sink IAV, IAVs of temperature and precipitation timeseries were also calculated using this method.

To quantify CO_2 effects on carbon sink, a relativized β-factor [*Walker et al.*, 2020] was used, which is represented as:

$$\beta = \ln(NBP_e/NBP_a)/\ln(CO_{2,e}/CO_{2,a}) \quad (1)$$

where NBP_e and NBP_a are NBP values at higher CO_2 concentration ($CO_{2,e}$) and lower CO_2 concentration ($CO_{2,a}$), respectively. The β-factor algorithm was applied to the decade mean values of CO_2 induced NBP changes (the difference between the RCP-CO_2 experiment and the RCP-Control experiment) during 2080-2089 and 2090-2099, under either RCP2.6 or RCP6.0. When β is less than 1, NBP tends to saturate, and *vice versa*. To quantify the long-term response of carbon sink to climate (temperature and precipitation), the multiple linear regression model regressing annual NBP against mean annual temperature and precipitation of land was applied to the climate only (RCP-Control) experiments [*Huntzinger et al.*, 2017]. Moreover, it was also applied to the experiments with varying CO_2 (RCP-CO_2) to check changes of response of carbon sink to climate, i.e., the interaction effects between CO_2 and climate.

We also adopted partial correlation analysis to partition impacts of climate variables on IAV of the terrestrial carbon sink, derived from the RCP-Control experiments. Meanwhile, to identify the major contributing area to both trends and IAVs of the terrestrial carbon sink, the global land was classified into six latitudinal bands, consisting of Boreal (≥ 55 °N), Northern Temperate (35 °N ~ 55 °N), Northern Subtropical (15 °N ~ 35 °N), Tropical (15 °S ~ 15 °N), Southern Subtropical (35 °S ~ 15 °S), and Southern Temperate (≥ 35 °S).

3 Results

3.1 Changes in NBP trend and IAV

The ensemble mean global NBP steadily increases before the 2040s under both RCP2.6 and 6.0, with its value changing from 0.96±0.44 Pg C yr^{-1} during 1986-2005 (well consistent with the contemporary estimate of 0.97±0.87 Pg C yr^{-1} by the Global Carbon Project [*Friedlingstein et al.*, 2019]) to 1.69±1.05 Pg C yr^{-1} (2040-2059) and 2.46±0.89 Pg C yr^{-1} (2040-2059), respectively, for each scenario (Fig. 1a). After that, NBP shows different trends under two RCPs (Fig. 1b). The terrestrial carbon sink gradually weakens to 0.60±0.71 Pg C yr^{-1} during 2080-2099 under RCP2.6 (Fig. 1a), coinciding with the concurrent gradual decrease of atmospheric CO_2 concentration (Fig. S1a). In contrast, under RCP6.0 NBP continues to grow (3.36±0.77 Pg C yr^{-1} during 2080-2099; Fig. 1a) until it reaches a peak around 2090 and then levels off or even slightly decreases (Fig. 1b) despite the linear increase of atmospheric CO_2 (Fig. S1a). According to the definition by *Canadell et al.* [2007], the two NBP trends are referred as "sink saturation" hereafter. Under RCP2.6, the decreased NBP rate compared to the historical period by the mid-century is found mainly in northwestern Amazon forest, central African tropical forest, part of tropical forests in Southeast Asia, and the southeast US (Fig. 2a). These NBP decreases spread further and are strengthened in the last 20 years of the century, covering almost the whole tropical forests, notably in the southeast Amazon forest, southeast US, part of western Europe, Australia, and high latitudes (Fig. 2b). The intensity of NBP reductions in high latitude regions, mainly found in Canada, Scandinavia, and western Russia, are second to those in tropical forests (Fig. 2b). Under RCP6.0, NBP in some pixels of Canada and western Russia is still negatively impacted but to a much smaller extent (Fig. 2c), particularly in western Russia where the signal of NBP change changes from the initial negative (decrease; Fig. 2c) to the final positive (increase; Fig. 2d). Tropical areas and high latitudes act as a major contributor to NBP increase as well as southwest and southeast China (Fig. 2d). Under either RCP2.6 or RCP6.0, the 17 ensemble members show a large spread in the NBP change, of which the order of the magnitude is approximately twice (RCP2.6) or half (RCP6.0) the value of the ensemble mean NBP by the end of the century (Fig. 1a). Such uncertainties primarily source from tropical areas, high latitudes and southwest and southeast China (Fig. S3). Moreover, the climate forcing induced uncertainty is larger than that induced by TBM differences (Figs. S4 and S5).

<Figure 1>

Because the sign of the NBP IAV can be positive or negative, IAV may offset each other among TBMs. We thus first calculated the IAV variances (in standard deviation, sd; the larger sd the stronger carbon flux anomaly) of individual ensemble member in a moving 20-year window and then calculated the ensemble mean of these IAV variances. The results show the global NBP IAV components under RCP2.6 and RCP6.0 are comparable (Fig. 1c), with the IAV variance of individual TBMs ranging from 1.45 Pg C yr^{-1} to 1.89 Pg C yr^{-1} and from 1.55 Pg C yr^{-1} to 2.10 Pg C yr^{-1} through 2006-2099, respectively. Under RCP2.6, the magnitude of NBP IAV variance is larger than the magnitude of the NBP trend (Figs. 1b and 1c). The NBP IAV is stronger under RCP6.0 than under RCP2.6, especially at the end of the century (Fig. 1d). Although the variance of global NBP IAV shows no significant temporal trend (stronger carbon sink if positive and vice versa, $p > 0.05$) across the whole period (1986-2099), large spatial divergences are found (Fig. S6). Several regions see smaller variance of NBP IAV than the historical period (1986-2005). These regions are mainly located in northern Amazon and Australia under RCP2.6 (Figs. S6a and S6b), where the same situation occurs under RCP6.0 by 2040-2059 (Fig. S6c). However, by the end of the century, these regions experience increase in variance of NBP IAV under RCP6.0 (Fig. S6d). In fact, across the majority of the globe, variance of NBP IAV is likely to increase under RCP6.0 (Fig. S6d).

<Figure 2>

3.2 Influencing factors for NBP changes

Although TBMs have a large spread on LUC effects relative to the absolute values (Figs. 3a and 3b), the ensemble mean shows LUC has a negative impact on NBP at the first several decades but afterwards consistently increases NBP under both RCPs (Figs. 3a and 3b). By the mid of the century (2040-2059), the land use change caused carbon sink is approximately neutral (0.09±0.09 Pg C yr^{-1}) under RCP2.6, while this neutral point occurs around 2060 under RCP6.0. By the end of the century (2080-2099), the land use change caused carbon sink under RCP2.6 and RCP6.0 is 0.44±0.05 Pg C yr^{-1} and 0.22±0.07 Pg C yr^{-1}, respectively. Across 2006-2009, the cumulative LUC contribution to NBP change under RCP2.6 and RCP6.0 is 10.32±40.43 Pg C and -3.38±31.55 Pg C, respectively (Fig. 3c).

<Figure 3>

The CO_2 effect is a major driver for terrestrial carbon sink increase under both RCP2.6 and RCP6.0, with its cumulative contribution to NBP change reaching 93.31±37.54 Pg C and 289.63±113.09 Pg C, respectively (Fig. 3c). However, under both RCPs the CO_2 effect is not always positive. Under RCP2.6, this occurs around the 2030s (Fig. 3a), closely following the atmospheric CO_2 concentration track (Fig. S1a). Under RCP6.0, the degradation occurs around the end of the 2080s (Fig. 3b) though the atmospheric CO_2 concentration continues growing (Fig. S1a). The decrease of the CO_2 effect under RCP2.6 even leads to a negative contribution to NBP change during 2080-2099 (-0.08±0.11 Pg C yr^{-1}; Fig. 3a and Table S2). The β-factor analysis shows that CO_2 effect on NBP saturates by the end century under RCP6.0. The CO_2 effect shows high spatial heterogeneity (Fig. 4). NBP in tropical forests shows the largest positive response to CO_2 increase, followed by other regions, such as the southeast US, southeast China, and high latitudes (Figs. 4a and 4c). However, when CO_2 gradually decreases in the second half of the century under RCP2.6, NBP in tropical area shows an obvious reduction compared to the control experiment (Fig. 4b) though the atmospheric CO_2 is still higher than in 2005 by the end of the century (Fig. S1a). In contrast, NBP in southeast US, southeast China, and high latitudes shows only minor decrease or even achieves slight increase (Fig. 4b). Under RCP6.0, NBP in high latitudes and tropical areas are mostly increased by elevated CO_2 (Figs. 4c and 4d), while ecosystems in arid or semi-arid regions, such as northwestern China, Central Asia, mid and west US, and inland Australia, consistently gain less NBP than other regions (Fig. 4). However, by the end century, CO_2 effects on NBP show saturation across a wide range of areas, such as tropical regions, mid-western US and Australia (Fig. 5).

<Figure 4>

<Figure 5>

We further investigate effects of climate on changes in NBP (Fig. 3). The cumulative climate effect on NBP is positive under RCP2.6 (18.29±65.93 Pg C), whereas it is negative under RCP6.0 (-52.21±90.17 Pg C). The temperature effect is the primary negative contributor to NBP changes under both RCPs (Fig. 6). Under RCP2.6, the negative effect of warming is widely distributed, especially in tropical and subtropical ecosystems, but only in part of high latitudes (Fig. 6). There are only a few regions where NBP shows positive response to temperature increase, including part of east Siberia, part of the Qinghai-Tibet Plateau and part of south Africa, but the 17 ensemble members have relatively low consistency (Fig. 6). Under RCP6.0, more areas show a negative response of NBP to temperature increase (Fig. 6). In contrast, increased precipitation generally stimulates NBP (Fig. 7). Compared to those relatively moist ecosystems, NBP in arid and semi-arid ecosystems shows higher positive sensitivity to precipitation (Fig. 7). A considerable fraction of high latitudes, in contrast, shows negative but weak responses to precipitation, mainly in Siberia and east Canada, though the 17 ensemble members show low consistency (Fig. 7). Additionally, we find that elevated CO_2 may (ensemble members show low consistency) decrease the NBP sensitivity to temperature in low and mid-latitudes, particularly in tropical and subtropical areas, but increase it in high latitudes (Figs. S7 and S9). The NBP sensitivity to precipitation is widely increased by elevated CO_2 in areas with low water availability or seasonal water deficit, such as inland Australia, Central Asia, and mid-west U.S., but decreased in relatively moist areas (Figs. S8 and S10).

<Figure 6>

<Figure 7>

3.3 Component fluxes of NBP

The interannual variation in NBP is highly correlated (R^2=0.58 and R^2=0.82 under RCP2.6 and RCP6.0, respectively) with the dynamics of GPP and Re changes (Fig. S11). Figure 8 shows under RCP6.0, climate change increased Re more than GPP, leading to NBP reduction. Both elevated CO_2 and land use change stimulate GPP and Re, with the former increased more (Fig. 8). Spatially, Ecosystems in arid and semi-arid regions show much less GPP increase than those in moist regions (Fig. 9). There are manifest spatial differences within high latitudes, with northern North America, Europe and west Siberia gaining higher GPP growth and east Siberia lower (Fig. 9). Under RCP2.6, it is noted that contrary to most of the world, GPP in Australia decreases considerably by the end of the century (Fig. 9b). Of all factors, warming is the major negative contributor to GPP, widely distributed in the warming regions like Southern Hemisphere and low latitudes of the Northern Hemisphere (Fig. S12). The negative effect of increased precipitation on GPP is concentrated in high latitudes but with low consistency of the 17 ensemble members (Fig.

S13). Ecosystem respiration shows similar spatial patterns to GPP in its temporal changes and responses to warming and precipitation under both RCPs (Figs. S14-S16). But ecosystem respiration generally has lower sensitivity in lower latitudes and higher sensitivity in high latitudes to temperature (Figs. S12 and S15). In contrast, ecosystem respiration shows lower sensitivity to precipitation than GPP (Figs. S13 and S16).

<Figure 8>

<Figure 9>

3.4 Influencing factors for NBP IAV

<Figure 10>

The partial correlation analysis shows global NBP IAV was jointly controlled by the positive effect of precipitation and the negative impact of temperature (Fig. 10). Under RCP2.6, the correlation of temperature with global NBP IAV is stronger than that of precipitation in most time, whereas it is the opposite under RCP6.0 (Fig. 10). During 1986-2005, temperature showed wide negative correlation with NBP IAV, particularly in low latitudes like northwestern Amazon forest, except in high latitudes and part of the Qinghai-Tibet Plateau, where temperature showed weak to moderate positive impacts (Fig. 11a). Under RCP2.6 and RCP6.0, more area shows the negative impact of temperature on NBP IAV (Figs. 11c and 11e). Precipitation showed generally positive correlation with NBP IAV in history, notably in arid or semi-arid ecosystems or those with seasonally dry climate, but weak negative impact in northern Asia and eastern Canada (Fig. 11b). The positive impact of precipitation on NBP IAV degrades in Africa but strengthens in Eurasia under both RCP2.6 and RCP6.0 by the end of the century (Figs. 11d and 11f). The latitudinal patterns show that tropical NBP IAV is the most correlated with temperature and precipitation under both RCPs, while NBP IAV in boreal area shows slight response to climate variability (Fig. S17).

<Figure 11>

4 Discussion

4.1 LUC-caused carbon sink

Land use change, such as deforestation [*Qie et al.*, 2017] and reforestation [*Kondo et al.*, 2018; *Thomas A. M. Pugh et al.*, 2019] as well as land management [*Erb et al.*, 2018], can reduce or increase the terrestrial carbon sink regionally. The higher LUC-caused carbon sink under RCP2.6 than RCP6.0 suggests that large-scale bioenergy croplands could help sequester carbon from the atmosphere, as there is less food cropland under RCP2.6 than RCP6.0 (Fig. S1). However, large spread between TBM estimates (Fig. 3) prompts that there exists substantial uncertainty in model representations of LUC related to bioenergy croplands (Table S1). Current TBMs mostly adopt a bookkeeping method to account for deforestation, which depends on limited field observations of carbon storage dynamics during deforestation and could not fully account for spatial heterogeneity in carbon loss during land conversion. Several studies also argued that the negative LUC impacts might have been substantially underestimated due to lack of sufficient sampling in subsoil [*Don et al.*, 2011] and lack of consideration of tree harvesting and land clearing from shifting cultivation by TBMs [*Arneth et al.*, 2017]. Furthermore, most TBMs of this study lack full representations of agricultural management options in the new converted farmlands (Table S1), such as cropping practices, irrigation, fertilizer application and tillage, which can significantly affect the remaining soil organic carbon [*Houghton*, 2010]. Specifically, three models (LPJ-GUESS, LPJmL, and ORCHIDEE) explicitly include bioenergy cropland types, of which only one (LPJmL) partitions bioenergy cropland into trees and grasslands while the other two only include C3/C4 grassland or crop types. Two models (LPJmL and ORCHIDEE) consider bioenergy cropland harvest, whereas none of the TBMs account for wood harvest (Table S1). Except ORCHIDEE, the TBMs do not include tillage impacts on soil organic carbon. Of the two models with N limits, the version of LPJ-GUESS used in this study does not consider N fertilizer application. Therefore, whether and to which extent bioenergy cropland expansion can increase terrestrial carbon sink need further investigation.

4.2 CO_2-caused carbon sink

The CO_2 effect on terrestrial carbon sink is one of the largest negative feedbacks to climate warming. As much as 60% of the contemporary terrestrial sink compared with that in 1850 may be explained by the increasing atmospheric CO_2 concentration [*Schimel et al.*, 2015]. The CO_2-caused sink depends on the balance between carbon uptake by CO_2 fertilization effects and carbon emissions by ecosystem respiration. The CO_2 fertilization effect can be limited by climate factors, and is most pronounced in the tropics, followed by northern mid-latitudes and boreal latitudes [*O'Sullivan et al.*, 2019; *Schimel et al.*, 2015; *Sitch et al.*, 2015]. Ecosystem respiration is mainly regulated by temperature, water availability, microbial activity and carbon substrate [*Davidson et al.*, 1998; *Migliavacca et al.*, 2011]. Our results on historical CO_2 effects on NBP are consistent with previous studies and suggest that tropical areas, southeast China, southeast US and boreal areas show significant enhancement in NBP [*O'Sullivan et al.*, 2019; *Sitch et al.*, 2015]. The result under RCP2.6 that the CO_2-caused carbon sink will eventually weaken when CO_2 concentration declines, is analogous to the simulations by Earth system models under negative emissions [*Jones et al.*, 2016]. The reason lies in that the decrease of decomposition of accumulated carbon storage lags behind GPP decrease, which has been reported at even an hourly time-scale [*Han et al.*, 2014]. For those models with nitrogen cycling, decreased CO_2 fertilization effects may keep more nitrogen in soil, which can stimulate soil organic matter decomposition [e.g., *Chen et al.*, 2018]. But most importantly, our result under RCP6.0 reveals that CO_2 effect on carbon sink would saturate, suggesting the negative feedback of terrestrial ecosystems to climate warming has its upper threshold. In addition, the CO_2-caused carbon sink may be further limited by nutrient availability, such as nitrogen limitation in high latitudes [*Du et al.*, 2020; *Y P Wang et al.*, 2011] and phosphorous in tropical regions [*Du et al.*, 2020; *Goll et al.*, 2018; *Y P Wang et al.*, 2011]. Therefore, when considering these limits, the CO_2-caused carbon sink would likely be weakened, resulting in earlier carbon sink saturation, because most TBMs used in this study do not couple nutrient cycles with carbon cycle.

4.3 Climate-caused carbon sink changes

The increasing trend of the terrestrial carbon sink since 1980 is attributed to precipitation stimulation of vegetation growth and expansion of semi-arid ecosystems as well as temperature effects [*Poulter et al.*, 2014; *Poulter et al.*, 2013]. Projections using Earth System Models also suggested that the future land carbon sink could be reduced by drying trends [*Green et al.*, 2019]. Our results are consistent with these studies in a sense that global terrestrial carbon sink is positively and closely correlated with precipitation. However, our study suggests that in the future, the negative impacts of temperature are likely to dominate, consistent with previous studies [e.g., *Yuan et al.*, 2021], as primary production is extremely sensitive to heat stress [*Allakhverdiev et al.*, 2008]. When ambient temperature is lower than the optimal temperature for ecosystem productivity, warming would enhance GPP but meanwhile may promote decomposition of soil organic carbon. When ambient temperature exceeds the optimal for photosynthesis, warming would weaken GPP while ecosystem respiration would increase further [*Niu et al.*, 2012; *Yvon-Durocher et al.*, 2010]. Such theoretical derivations are reflected in our estimated NBP sensitivity to temperature, particularly in tropical area where the growing-season temperature has already approached the ecosystem optimal temperature [*Corlett*, 2011; *Doughty and Goulden*, 2008; *Sullivan et al.*, 2020]. There has been much research on temperature optima for ecosystem production at various spatial scales [e.g., *Huang et al.*, 2019; *Sullivan et al.*, 2020] but we have only limited reports on its counterpart for NBP [*Niu et al.*, 2012], estimation of which will help improve projecting the future carbon cycle. The sensitivities of NBP to temperature and precipitation can also be mediated by each other or other environmental factors. In a multi-model study (in which several TBMs of this study also participated) of ENSO impacts on tropical carbon sink, *Fang et al.* [2017] reported that the sensitivity of terrestrial carbon sink to temperature and precipitation is impacted by prevalent climate conditions and precipitation may influence temperature response of GPP, while models failed to capture these functions. Likewise, there may be some uncertainty on our results of the minor or moderate impacts of CO_2 increase on temperature sensitivity of NBP, because most TBMs here actually do not consider CO_2 effects on carbon allocation [Table S1, *Jiang et al.*, 2020; *T. A. M. Pugh et al.*, 2016], which provides carbon substrate for ecosystem respiration. The significant CO_2 impact on precipitation response of NBP could be attributed to the "water-saving" effect of elevated CO_2, which reduces stomatal conductance and thus water demand by plants for equivalent photosynthesis [*Ainsworth and Rogers*, 2007].

4.4 Drivers of NBP IAV

Among biomes, some studies employing atmospheric inversions attributed the most of land carbon sink IAV to moist tropical forests. Yet *Ahlstrom et al.* [2015] rather related the dominant role of semi-arid ecosystems during 1982-2011 to both temperature and precipitation through investigation by TBMs and upscaled flux measurements. Apparently, the controversial points focus on the contribution of tropical forests *vs*. semi-arid ecosystems and the impact of temperature *vs*. precipitation. A reconciling effort by *Jung et al.* [2017] found that temperature governs globally due to compensatory effects of water availability at local and global scales. In contrast, based on multiple lines of evidence from observations and models, *Piao et al.* [2020] described emerging interaction effects between temperature and water availability on carbon cycle IAV.

Simultaneously, they suggested that tropical ecosystems dominate terrestrial carbon sink IAV from 1980 and all other tropical ecosystems contribute as much as the tropical semi-arid ecosystems. Our results for the historical period are consistent with *Ahlstrom et al.* [2015] and *Piao et al.* [2020] in a sense that temperature and precipitation jointly control the NBP IAV but with the importance of temperature increasing in the first several decades under RCP6.0 (Fig. 10). Moreover, the correlation between tropical NBP IAV and climate variables suggest that tropical climate change could potentially significantly influence the global NBP IAV, considering tropical NBP is a major part of global NBP.

4.5 Outlook for TBMs, field experiments, and policies

Not all TBMs in this study consider impacts of fire and photosynthetic acclimation to warming (Table S1), the latter of which is critical for tropical and boreal forests where ecosystems store the largest fraction of biomass and soil carbon and massive mortality or dieback may arise from heat and drought stress [*Huang et al.*, 2019; *Ito et al.*, 2020]. Recent big fires in Amazon and Australia have attracted much attention. According to the Global Fire Emissions Database (https://www.globalfiredata.org/), total carbon emissions from forest fires rose by 26% in 2019 than the previous year, which constitute a drastic carbon sink anomaly though the absolute emission value did not exceed the long-term average too much. Moreover, fires in boreal area may alter vegetation composition [*Turner et al.*, 2019], resulting in long-term footprint on carbon cycle. Likewise, forest disturbances and their interactions are likely to increase under climate change [*Seidl et al.*, 2017] and have shown the potential to reduce carbon stocks [*Kurz et al.*, 2008; *Seidl et al.*, 2014]. These processes should be incorporated into TBMs.

Experiments of CO_2 fertilization effects are essentially required, particularly outside the temperate regions, where most current FACE experiments are located [*Norby and Zak*, 2011]. Analysis or integration of experiments on interaction effects of various factors that are distributed globally would help improve understanding the underlying mechanisms for impacting carbon cycle and TBMs' performance.

The comparison between carbon sinks under RCP2.6 and RCP6.0 suggest that higher atmospheric CO_2 concentration could result in a larger carbon sink due to the larger CO_2 fertilization effect. However, simultaneously there would be stronger, negative climate feedback that higher warming would reduce carbon sink more and increase the amplitude of carbon extremes. This brings discussion on tipping points of various ecosystems into scope. Warming or droughts induced tree mortality [*McDowell and Allen*, 2015; *Van Mantgem et al.*, 2009] or permafrost thawing [*Burke et al.*, 2018; *Chadburn et al.*, 2017] could trigger a series of ramifications like more fires and insect outbreaks. The saturation of the terrestrial carbon sink under the no-mitigation scenario RCP6.0 indicates that the role of terrestrial ecosystems in mediating climate change would be weakened in future, and active mitigation efforts like reducing fossil fuel combustion and industrial emissions as assumed under RCP2.6 are necessary. Otherwise, further warming and the declined CO_2 effects on carbon sink may have the potential to eventually turn the terrestrial biosphere into a carbon source [*Canadell et al.*, 2007], which would exacerbate climate warming and cause further damage to both human and natural systems.

Acknowledgments

This study has been supported partially by National Science Foundation (Award number 1903722); National Key R & D Program of China (grant nos. 2017YFA0604702); the German Federal Ministry of Education and Research (BMBF, Grant No. 01LS1711A); the Climate Change Adaptation Research Program of National Institute for Environmental Studies, Japan; the European Commission "CASCADES Horizon 2020" (grant agreement 821010); Andrew Carnegie Fellowship (Award no. G-F-19-56910). The Inter-Sectoral Impact Model Intercomparison Project (ISIMIP) is funded through the German Federal Ministry of Education and Research (BMBF, Grant No. 01LS1711A). All data can be publicly accessed at https://esg.pik-potsdam.de/projects/isimip2b/. The statements made and views expressed are solely the responsibility of the authors.

References

Ahlstrom, A., et al. (2015), The dominant role of semi-arid ecosystems in the trend and variability of the land CO_2 sink, *Science*, *348*(6237), 895-899.

Ainsworth, E. A., and A. Rogers (2007), The response of photosynthesis and stomatal conductance to rising [CO_2]: mechanisms and environmental interactions, *Plant, cell & environment*, *30*(3), 258-270.

Allakhverdiev, S. I., V. D. Kreslavski, V. V. Klimov, D. A. Los, R. Carpentier, and P. Mohanty (2008), Heat stress: an overview of molecular responses in photosynthesis, *Photosynthesis research*, *98*(1), 541-550.

Anderegg, W. R. L., et al. (2015), Tropical nighttime warming as a dominant driver of variability in the terrestrial carbon sink, *Proceedings of the National Academy of Sciences*, *112*(51), 15591-15596.

Arneth, A., et al. (2017), Historical carbon dioxide emissions caused by land-use changes are possibly larger than assumed, *Nature Geoscience*, *10*(2), 79-84.

Ballantyne, A., C. Alden, J. Miller, P. Tans, and J. White (2012), Increase in observed net carbon dioxide uptake by land and oceans during the past 50 years, *Nature*, *488*(7409), 70-72.

Bastos, A., et al. (2020), Sources of Uncertainty in Regional and Global Terrestrial CO_2 Exchange Estimates, *Global Biogeochemical Cycles*, *34*(2), e2019GB006393.

Bondeau, A., P. C. Smith, S. Zaehle, S. Schaphoff, W. Lucht, W. Cramer, D. Gerten, H. LOTZE-CAMPEN, C. Müller, and M. Reichstein (2007), Modelling the role of agriculture for the 20th century global terrestrial carbon balance, *Global Change Biology*, *13*(3), 679-706.

Brienen, R. J., O. L. Phillips, T. R. Feldpausch, E. Gloor, T. R. Baker, J. Lloyd, G. Lopez-Gonzalez, A. Monteagudo-Mendoza, Y. Malhi, and S. L. Lewis (2015), Long-term decline of the Amazon carbon sink, *Nature*, *519*(7543), 344-348.

Burke, E. J., S. E. Chadburn, C. Huntingford, and C. D. Jones (2018), CO_2 loss by permafrost thawing implies additional emissions reductions to limit warming to 1.5 or 2 °C, *Environmental Research Letters*, *13*(2), 024024.

Canadell, J. G., D. E. Pataki, R. Gifford, R. A. Houghton, Y. Luo, M. R. Raupach, P. Smith, and W. Steffen (2007), Saturation of the Terrestrial Carbon Sink, in *Terrestrial Ecosystems in a Changing World*, edited by J. G. Canadell, D. E. Pataki and L. F. Pitelka, pp. 59-78, Springer Berlin Heidelberg, Berlin, Heidelberg.

Chadburn, S., E. Burke, P. Cox, P. Friedlingstein, G. Hugelius, and S. Westermann (2017), An observation-based constraint on permafrost loss as a function of global warming, *Nature Climate Change*, *7*(5), 340-344.
Chang, J., P. Ciais, X. Wang, S. Piao, G. Asrar, R. Betts, F. Chevallier, M. Dury, L. François, and K. Frieler (2017), Benchmarking carbon fluxes of the ISIMIP2a biome models, *Environmental Research Letters*, *12*(4), 045002.
Chen, Z., Y. Xu, Y. He, X. Zhou, J. Fan, H. Yu, and W. Ding (2018), Nitrogen fertilization stimulated soil heterotrophic but not autotrophic respiration in cropland soils: A greater role of organic over inorganic fertilizer, *Soil Biology and Biochemistry*, *116*, 253-264.
Corlett, R. T. (2011), Impacts of warming on tropical lowland rainforests, *Trends in ecology & evolution*, *26*(11), 606-613.
Cox, P. M., D. Pearson, B. B. Booth, P. Friedlingstein, C. Huntingford, C. D. Jones, and C. M. Luke (2013), Sensitivity of tropical carbon to climate change constrained by carbon dioxide variability, *Nature*, *494*(7437), 341-344.
Davidson, E. A., E. Belk, and R. D. Boone (1998), Soil water content and temperature as independent or confounded factors controlling soil respiration in a temperate mixed hardwood forest, *Global change biology*, *4*(2), 217-227.
Dietrich, J. P., et al. (2019), MAgPIE 4 – a modular open-source framework for modeling global land systems, *Geosci. Model Dev.*, *12*(4), 1299-1317.
Don, A., J. Schumacher, and A. Freibauer (2011), Impact of tropical land-use change on soil organic carbon stocks – a meta-analysis, *Global Change Biology*, *17*(4), 1658-1670.
Donohue, R. J., M. L. Roderick, T. R. McVicar, and G. D. Farquhar (2013), Impact of CO_2 fertilization on maximum foliage cover across the globe's warm, arid environments, *Geophysical Research Letters*, *40*(12), 3031-3035.
Doughty, C. E., and M. L. Goulden (2008), Are tropical forests near a high temperature threshold?, *Journal of Geophysical Research: Biogeosciences*, *113*(G1).
Du, E., C. Terrer, A. F. A. Pellegrini, A. Ahlström, C. J. van Lissa, X. Zhao, N. Xia, X. Wu, and R. B. Jackson (2020), Global patterns of terrestrial nitrogen and phosphorus limitation, *Nature Geoscience*, *13*(3), 221-226.
Erb, K.-H., et al. (2018), Unexpectedly large impact of forest management and grazing on global vegetation biomass, *Nature*, *553*(7686), 73-76.
Fang, Y., A. M. Michalak, C. R. Schwalm, D. N. Huntzinger, J. A. Berry, P. Ciais, S. Piao, B. Poulter, J. B. Fisher, and R. B. Cook (2017), Global land carbon sink response to temperature and precipitation varies with ENSO phase, *Environmental Research Letters*, *12*(6), 064007.
Fleischer, K., et al. (2019), Amazon forest response to CO_2 fertilization dependent on plant phosphorus acquisition, *Nature Geoscience*, *12*(9), 736-741.
Friedlingstein, P., M. Jones, M. O'Sullivan, R. Andrew, J. Hauck, G. Peters, W. Peters, J. Pongratz, S. Sitch, and C. Le Quéré (2019), Global carbon budget 2019, *Earth System Science Data*, *11*(4), 1783-1838.
Frieler, K., S. Lange, F. Piontek, C. P. Reyer, J. Schewe, L. Warszawski, F. Zhao, L. Chini, S. Denvil, and K. Emanuel (2017), Assessing the impacts of 1.5 °C global warming–simulation protocol of the Inter-Sectoral Impact Model Intercomparison Project (ISIMIP2b), *Geoscientific Model Development*, *10*(12), 4321.
Friend, A. D., W. Lucht, T. T. Rademacher, R. Keribin, R. Betts, P. Cadule, P. Ciais, D. B. Clark, R. Dankers, and P. D. Falloon (2014), Carbon residence time dominates uncertainty in terrestrial

vegetation responses to future climate and atmospheric CO_2, *Proceedings of the National Academy of Sciences*, *111*(9), 3280-3285.

Girardin, M. P., O. Bouriaud, E. H. Hogg, W. Kurz, N. E. Zimmermann, J. M. Metsaranta, R. de Jong, D. C. Frank, J. Esper, and U. Büntgen (2016), No growth stimulation of Canada's boreal forest under half-century of combined warming and CO_2 fertilization, *Proceedings of the National Academy of Sciences*, *113*(52), E8406-E8414.

Goll, D. S., E. Joetzjer, M. Huang, and P. Ciais (2018), Low phosphorus availability decreases susceptibility of tropical primary productivity to droughts, *Geophysical Research Letters*, *45*(16), 8231-8240.

Green, J. K., S. I. Seneviratne, A. M. Berg, K. L. Findell, S. Hagemann, D. M. Lawrence, and P. Gentine (2019), Large influence of soil moisture on long-term terrestrial carbon uptake, *Nature*, *565*(7740), 476.

Guimberteau, M., D. Zhu, F. Maignan, Y. Huang, C. Yue, S. Dantec-Nédélec, C. Ottlé, A. Jornet-Puig, A. Bastos, and P. Laurent (2018), ORCHIDEE-MICT (v8. 4.1), a land surface model for the high latitudes: model description and validation.

Han, G., Y. Luo, D. Li, J. Xia, Q. Xing, and J. Yu (2014), Ecosystem photosynthesis regulates soil respiration on a diurnal scale with a short-term time lag in a coastal wetland, *Soil Biology and Biochemistry*, *68*, 85-94.

Hickler, T., A. Rammig, and C. Werner (2015), Modelling CO_2 impacts on forest productivity, *Current Forestry Reports*, *1*(2), 69-80.

Houghton, R. A. (2010), How well do we know the flux of CO_2 from land-use change?, *Tellus B*, *62*(5), 337-351.

Houghton, R. A., and A. A. Nassikas (2017), Global and regional fluxes of carbon from land use and land cover change 1850–2015, *Global Biogeochemical Cycles*, *31*(3), 456-472.

Huang, M., S. Piao, P. Ciais, J. Peñuelas, X. Wang, T. F. Keenan, S. Peng, J. A. Berry, K. Wang, and J. Mao (2019), Air temperature optima of vegetation productivity across global biomes, *Nature ecology & evolution*, *3*(5), 772-779.

Huntzinger, D. N., et al. (2017), Uncertainty in the response of terrestrial carbon sink to environmental drivers undermines carbon-climate feedback predictions, *Scientific Reports*, *7*(1), 4765.

Ito, A., and M. Inatomi (2012), Water-use efficiency of the terrestrial biosphere: a model analysis focusing on interactions between the global carbon and water cycles, *Journal of Hydrometeorology*, *13*(2), 681-694.

Ito, A., C. P. Reyer, A. Gädeke, P. Ciais, J. Chang, M. Chen, L. François, M. Forrest, T. Hickler, and S. Ostberg (2020), Pronounced and unavoidable impacts of low-end global warming on northern high-latitude land ecosystems, *Environmental Research Letters*, *15*(4), 044006.

Janssens, I., W. Dieleman, S. Luyssaert, J.-A. Subke, M. Reichstein, R. Ceulemans, P. Ciais, A. J. Dolman, J. Grace, and G. Matteucci (2010), Reduction of forest soil respiration in response to nitrogen deposition, *Nature geoscience*, *3*(5), 315-322.

Jiang, M., B. E. Medlyn, J. E. Drake, R. A. Duursma, I. C. Anderson, C. V. Barton, M. M. Boer, Y. Carrillo, L. Castaneda-Gomez, and L. Collins (2020), The fate of carbon in a mature forest under carbon dioxide enrichment, *Nature*, *580*(7802), 227-231.

Jones, C. D., P. Ciais, S. J. Davis, P. Friedlingstein, T. Gasser, G. P. Peters, J. Rogelj, D. P. van Vuuren, J. G. Canadell, and A. Cowie (2016), Simulating the Earth system response to negative emissions, *Environmental Research Letters*, *11*(9), 095012.

Jung, M., M. Reichstein, C. R. Schwalm, C. Huntingford, S. Sitch, A. Ahlström, A. Arneth, G. Camps-Valls, P. Ciais, and P. Friedlingstein (2017), Compensatory water effects link yearly global land CO_2 sink changes to temperature, *Nature*, *541*(7638), 516-520.
Keeling, C. D., T. P. Whorf, M. Wahlen, and J. van der Plichtt (1995), Interannual extremes in the rate of rise of atmospheric carbon dioxide since 1980, *Nature*, *375*(6533), 666-670.
Kondo, M., K. Ichii, P. K. Patra, B. Poulter, L. Calle, C. Koven, T. A. Pugh, E. Kato, A. Harper, and S. Zaehle (2018), Plant regrowth as a driver of recent enhancement of terrestrial CO2 uptake, *Geophysical Research Letters*, *45*(10), 4820-4830.
Kondo, M., et al. (2020), State of the science in reconciling top-down and bottom-up approaches for terrestrial CO_2 budget, *Global Change Biology*, *26*(3), 1068-1084.
Kurz, W. A., C. C. Dymond, G. Stinson, G. J. Rampley, E. T. Neilson, A. L. Carroll, T. Ebata, and L. Safranyik (2008), Mountain pine beetle and forest carbon feedback to climate change, *Nature*, *452*(7190), 987-990.
Le Quéré, C., R. M. Andrew, P. Friedlingstein, S. Sitch, J. Hauck, J. Pongratz, P. A. Pickers, J. I. Korsbakken, G. P. Peters, and J. G. Canadell (2018), Global carbon budget 2018, *Earth System Science Data*, *10*(4), 2141-2194.
McDowell, N. G., and C. D. Allen (2015), Darcy's law predicts widespread forest mortality under climate warming, *Nature Climate Change*, *5*(7), 669-672.
Medlyn, B. E., S. Zaehle, M. G. De Kauwe, A. P. Walker, M. C. Dietze, P. J. Hanson, T. Hickler, A. K. Jain, Y. Luo, and W. Parton (2015), Using ecosystem experiments to improve vegetation models, *Nature Climate Change*, *5*(6), 528-534.
Migliavacca, M., M. Reichstein, A. D. Richardson, R. Colombo, M. A. Sutton, G. Lasslop, E. Tomelleri, G. Wohlfahrt, N. Carvalhais, and A. Cescatti (2011), Semiempirical modeling of abiotic and biotic factors controlling ecosystem respiration across eddy covariance sites, *Global Change Biology*, *17*(1), 390-409.
Nadelhoffer, K. J., B. A. Emmett, P. Gundersen, O. J. Kjønaas, C. J. Koopmans, P. Schleppi, A. Tietema, and R. F. Wright (1999), Nitrogen deposition makes a minor contribution to carbon sequestration in temperate forests, *Nature*, *398*(6723), 145-148.
Niu, S., Y. Luo, S. Fei, W. Yuan, D. Schimel, B. E. Law, C. Ammann, M. Altaf Arain, A. Arneth, and M. Aubinet (2012), Thermal optimality of net ecosystem exchange of carbon dioxide and underlying mechanisms, *New Phytologist*, *194*(3), 775-783.
Norby, R. J., and D. R. Zak (2011), Ecological lessons from free-air CO_2 enrichment (FACE) experiments, *Annual review of ecology, evolution, and systematics*, *42*, 181-203.
O'Sullivan, M., D. V. Spracklen, S. A. Batterman, S. R. Arnold, M. Gloor, and W. Buermann (2019), Have Synergies Between Nitrogen Deposition and Atmospheric CO_2 Driven the Recent Enhancement of the Terrestrial Carbon Sink?, *Global biogeochemical cycles*, *33*(2), 163-180.
Pan, N., X. Feng, B. Fu, S. Wang, F. Ji, and S. Pan (2018), Increasing global vegetation browning hidden in overall vegetation greening: Insights from time-varying trends, *Remote Sensing of Environment*, *214*, 59-72.
Piao, S., X. Wang, K. Wang, X. Li, A. Bastos, J. G. Canadell, P. Ciais, P. Friedlingstein, and S. Sitch (2020), Interannual variation of terrestrial carbon cycle: Issues and perspectives, *Global Change Biology*, *26*(1), 300-318.
Poulter, B., D. Frank, P. Ciais, R. B. Myneni, N. Andela, J. Bi, G. Broquet, J. G. Canadell, F. Chevallier, and Y. Y. Liu (2014), Contribution of semi-arid ecosystems to interannual variability of the global carbon cycle, *Nature*, *509*(7502), 600-603.

Poulter, B., et al. (2013), Recent trends in Inner Asian forest dynamics to temperature and precipitation indicate high sensitivity to climate change, *Agricultural and Forest Meteorology*, *178-179*, 31-45.

Pugh, T. A. M., C. Müller, A. Arneth, V. Haverd, and B. Smith (2016), Key knowledge and data gaps in modelling the influence of CO_2 concentration on the terrestrial carbon sink, *Journal of Plant Physiology*, *203*, 3-15.

Pugh, T. A. M., M. Lindeskog, B. Smith, B. Poulter, A. Arneth, V. Haverd, and L. Calle (2019), Role of forest regrowth in global carbon sink dynamics, *Proceedings of the National Academy of Sciences*, *116*(10), 4382-4387.

Qie, L., S. L. Lewis, M. J. Sullivan, G. Lopez-Gonzalez, G. C. Pickavance, T. Sunderland, P. Ashton, W. Hubau, K. A. Salim, and S.-I. Aiba (2017), Long-term carbon sink in Borneo's forests halted by drought and vulnerable to edge effects, *Nature communications*, *8*(1), 1966.

Reay, D. S., F. Dentener, P. Smith, J. Grace, and R. A. Feely (2008), Global nitrogen deposition and carbon sinks, *Nature Geoscience*, *1*(7), 430-437.

Schimel, D., B. B. Stephens, and J. B. Fisher (2015), Effect of increasing CO_2 on the terrestrial carbon cycle, *Proceedings of the National Academy of Sciences*, *112*(2), 436-441.

Seidl, R., M.-J. Schelhaas, W. Rammer, and P. J. Verkerk (2014), Increasing forest disturbances in Europe and their impact on carbon storage, *Nature Climate Change*, *4*(9), 806-810.

Seidl, R., et al. (2017), Forest disturbances under climate change, *Nature Climate Change*, *7*(6), 395-402.

Sitch, S., P. Friedlingstein, N. Gruber, S. D. Jones, G. Murray-Tortarolo, A. Ahlström, S. C. Doney, H. Graven, C. Heinze, and C. Huntingford (2015), Recent trends and drivers of regional sources and sinks of carbon dioxide, *Biogeosciences*, *12*(3), 653-679.

Smith, B., D. Warlind, A. Arneth, T. Hickler, P. Leadley, J. Siltberg, and S. Zaehle (2014), Implications of incorporating N cycling and N limitations on primary production in an individual-based dynamic vegetation model, *Biogeosciences*, *11*, 2027-2054.

Smith, K. W., S. C. Reed, C. C. Cleveland, A. P. Ballantyne, W. R. L. Anderegg, W. R. Wieder, Y. Y. Liu, and S. W. Running (2016), Large divergence of satellite and Earth system model estimates of global terrestrial CO_2 fertilization, *Nature Climate Change*, *6*(3), 306-310.

Sullivan, M. J. P., et al. (2020), Long-term thermal sensitivity of Earth's tropical forests, *Science*, *368*(6493), 869-874.

Tagesson, T., et al. (2020), Recent divergence in the contributions of tropical and boreal forests to the terrestrial carbon sink, *Nature Ecology & Evolution*, *4*(2), 202-209.

Terrer, C., et al. (2019), Nitrogen and phosphorus constrain the CO_2 fertilization of global plant biomass, *Nature Climate Change*, *9*(9), 684-689.

Tian, H., J. M. Melillo, D. W. Kicklighter, A. D. McGuire, J. V. K. Helfrich, B. Moore, and C. J. Vörösmarty (1998), Effect of interannual climate variability on carbon storage in Amazonian ecosystems, *Nature*, *396*(6712), 664-667.

Tian, H., X. Xu, C. Lu, M. Liu, W. Ren, G. Chen, J. Melillo, and J. Liu (2011a), Net exchanges of CO_2, CH_4, and N_2O between China's terrestrial ecosystems and the atmosphere and their contributions to global climate warming, *Journal of Geophysical Research: Biogeosciences*, *116*(G2).

Tian, H., J. Melillo, C. Lu, D. Kicklighter, M. Liu, W. Ren, X. Xu, G. Chen, C. Zhang, and S. Pan (2011b), China's terrestrial carbon balance: contributions from multiple global change factors, *Global Biogeochemical Cycles*, *25*(1).

Trugman, A. T., D. Medvigy, J. S. Mankin, and W. R. L. Anderegg (2018), Soil Moisture Stress as a Major Driver of Carbon Cycle Uncertainty, *Geophysical Research Letters*, *45*(13), 6495-6503.

Turner, M. G., K. H. Braziunas, W. D. Hansen, and B. J. Harvey (2019), Short-interval severe fire erodes the resilience of subalpine lodgepole pine forests, *Proceedings of the National Academy of Sciences*, *116*(23), 11319-11328.

van der Molen, M. K., A. J. Dolman, P. Ciais, T. Eglin, N. Gobron, B. E. Law, P. Meir, W. Peters, O. L. Phillips, and M. Reichstein (2011), Drought and ecosystem carbon cycling, *Agricultural and Forest Meteorology*, *151*(7), 765-773.

Van Mantgem, P. J., N. L. Stephenson, J. C. Byrne, L. D. Daniels, J. F. Franklin, P. Z. Fulé, M. E. Harmon, A. J. Larson, J. M. Smith, and A. H. Taylor (2009), Widespread increase of tree mortality rates in the western United States, *Science*, *323*(5913), 521-524.

Walker, A. P., M. G. De Kauwe, A. Bastos, S. Belmecheri, K. Georgiou, R. Keeling, S. M. McMahon, B. E. Medlyn, D. J. Moore, and R. J. Norby (2020), Integrating the evidence for a terrestrial carbon sink caused by increasing atmospheric CO2, *New Phytologist*.

Wang, J., N. Zeng, and M. Wang (2016), Interannual variability of the atmospheric CO_2 growth rate: roles of precipitation and temperature, *Biogeosciences*, *13*(8).

Wang, K., Y. Wang, X. Wang, Y. He, X. Li, R. F. Keeling, P. Ciais, M. Heimann, S. Peng, and F. Chevallier (2020), Causes of slowing-down seasonal CO2 amplitude at Mauna Loa, *Global Change Biology*.

Wang, T., M. Zhang, Q. Yu, and H. Zhang (2012), Comparing the applications of EMD and EEMD on time–frequency analysis of seismic signal, *Journal of Applied Geophysics*, *83*, 29-34.

Wang, W., P. Ciais, R. R. Nemani, J. G. Canadell, S. Piao, S. Sitch, M. A. White, H. Hashimoto, C. Milesi, and R. B. Myneni (2013), Variations in atmospheric CO_2 growth rates coupled with tropical temperature, *Proceedings of the National Academy of Sciences*, *110*(32), 13061-13066.

Wang, Y. P., E. Kowalczyk, R. Leuning, G. Abramowitz, M. R. Raupach, B. Pak, E. van Gorsel, and A. Luhar (2011), Diagnosing errors in a land surface model (CABLE) in the time and frequency domains, *Journal of Geophysical Research: Biogeosciences*, *116*(G1).

Welch, J. R., J. R. Vincent, M. Auffhammer, P. F. Moya, A. Dobermann, and D. Dawe (2010), Rice yields in tropical/subtropical Asia exhibit large but opposing sensitivities to minimum and maximum temperatures, *Proceedings of the National Academy of Sciences*, *107*(33), 14562-14567.

Wigneron, J.-P., L. Fan, P. Ciais, A. Bastos, M. Brandt, J. Chave, S. Saatchi, A. Baccini, and R. Fensholt (2020), Tropical forests did not recover from the strong 2015–2016 El Niño event, *Science advances*, *6*(6), eaay4603.

Yuan, M., Q. Zhu, J. Zhang, J. Liu, H. Chen, C. Peng, P. Li, M. Li, M. Wang, and P. Zhao (2021), Global response of terrestrial gross primary productivity to climate extremes, *Science of The Total Environment*, *750*, 142337.

Yvon-Durocher, G., J. I. Jones, M. Trimmer, G. Woodward, and J. M. Montoya (2010), Warming alters the metabolic balance of ecosystems, *Philosophical Transactions of the Royal Society B: Biological Sciences*, *365*(1549), 2117-2126.

Table 1. ISIMIP2b biome sector simulation protocol

Experiment	Climate	Land use	CO_2
Historical	1861-2005	Historical	Historical
RCP2.6-Control	2006-2099 (RCP2.6)	2005	2005
RCP2.6-CO_2	2006-2099 (RCP2.6)	2005	RCP2.6
RCP2.6-LUC	2006-2099 (RCP2.6)	RCP2.6	RCP2.6
RCP6.0-Control	2006-2099 (RCP6.0)	2005	2005
RCP6.0-CO_2	2006-2099 (RCP6.0)	2005	RCP6.0
RCP6.0-LUC	2006-2099 (RCP6.0)	RCP6.0	RCP6.0

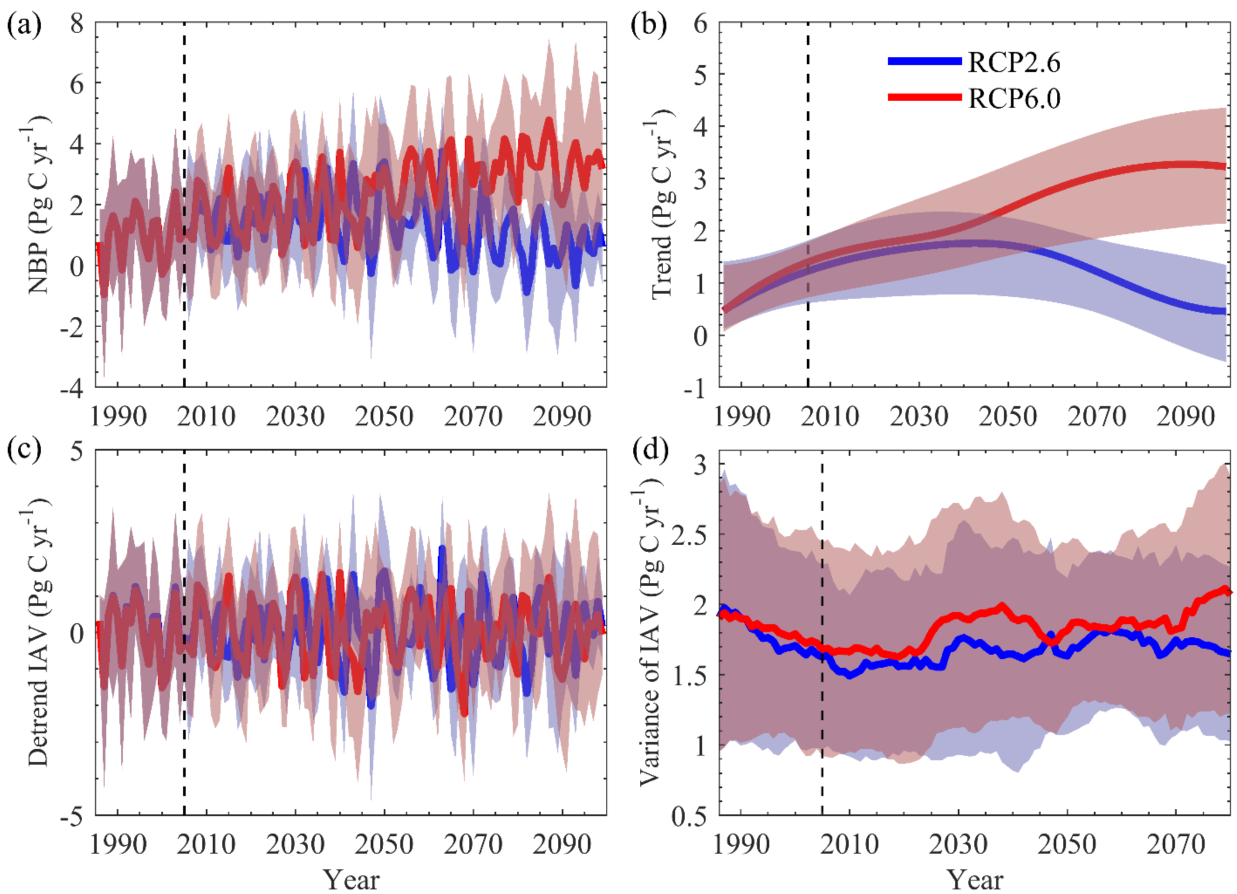

Figure 1. Ensemble mean of global annual NBP during 1986-2099. The total NBP (a) is partitioned into trend (b) and interannual variability (IAV, c) using the EEMD method. The variance (in standard deviation) of global NBP IAV (d) is calculated as the ensemble mean of standard deviations of NBP IAV time-series of individual TBMs in a moving 20-year window. Shaded areas represent standard deviations of results from all ensemble members under each representative concentration pathway (RCP). The dashed line indicates the year 2006. The *x* axis indicates the start year of the moving window in Figure 1d.

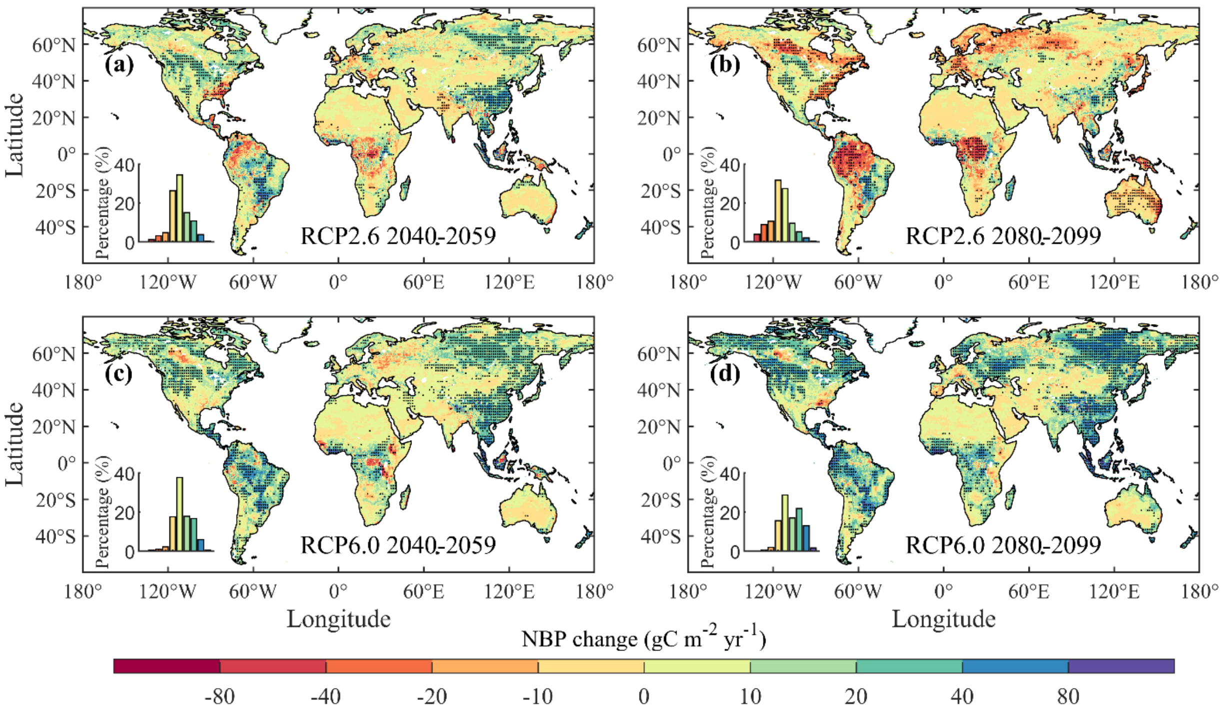

Figure 2. Spatial patterns of NBP changes calculated as the difference between the mean annual NBP during 2040-2059 (a, c) or 2080-2099 (b, d) in the RCP-LUC experiments under RCP2.6 (a, b) or RCP6.0 (c, d) and the mean annual NBP during 1986-2005. The insets show histograms of pixel values of NBP changes. The stippling pixels indicate that at least 80% of all the 17 ensemble members have the same sign for the NBP change.

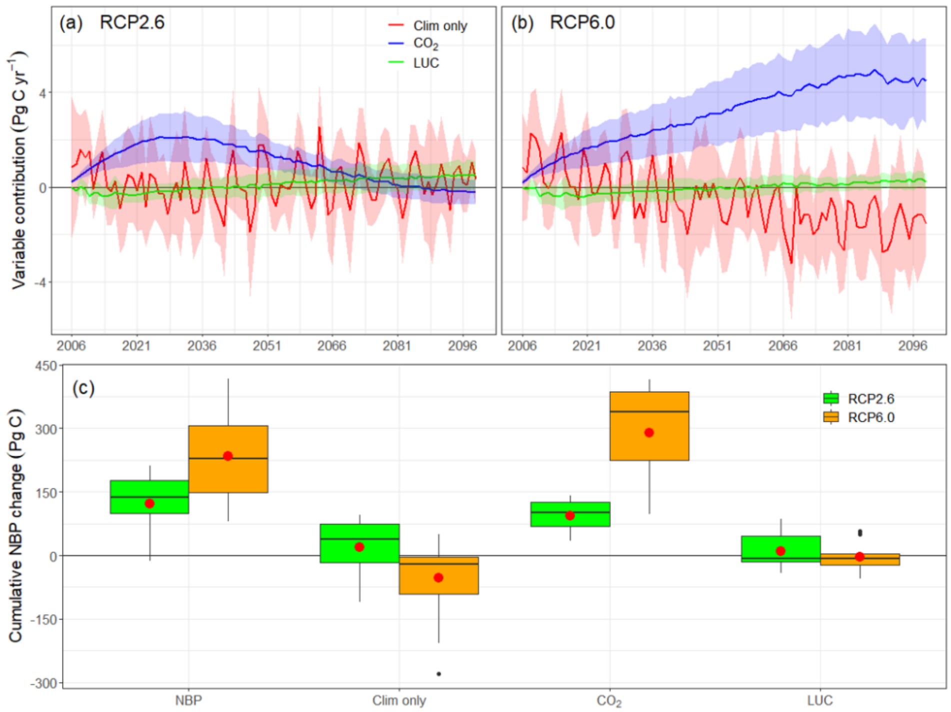

Figure 3. Attribution of the annual NBP to different factors (a and b) and the cumulative contribution of each factor during 2006-2099 (c). The black dots are outliers and the red dots indicate the ensemble mean of all simulations under each RCP (c). The whiskers indicate the minimum and maximum of all estimates, and the three horizontal lines of each box are the 25% quantile, median, and 75% quantile of all estimates (c). The one-sample *t*-test indicates all distributions are significantly different from zero (c).

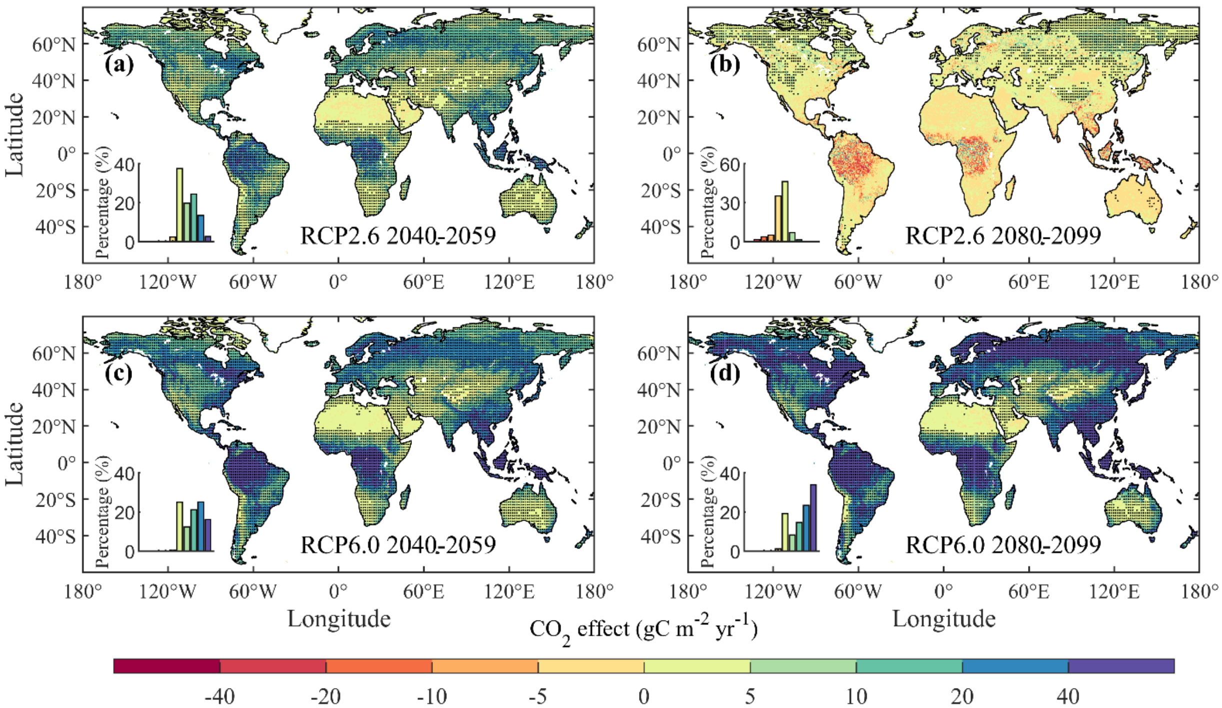

Figure 4. Spatial patterns of CO_2-caused NBP under RCP2.6 (a, b) and RCP6.0 (c, d) calculated as the difference between the mean annual NBP of all ensemble members of the RCP-CO_2 experiment with varying CO_2 during 2040-2059 (a, c) or 2080-2099 (b, d) and that of all ensemble members of the RCP-Control experiment with fixed CO_2. The insets show histograms of pixel values of CO_2-caused NBP. The stippling pixels indicate that at least 80% of all the 17 ensemble members have the same sign for the CO_2-caused NBP change.

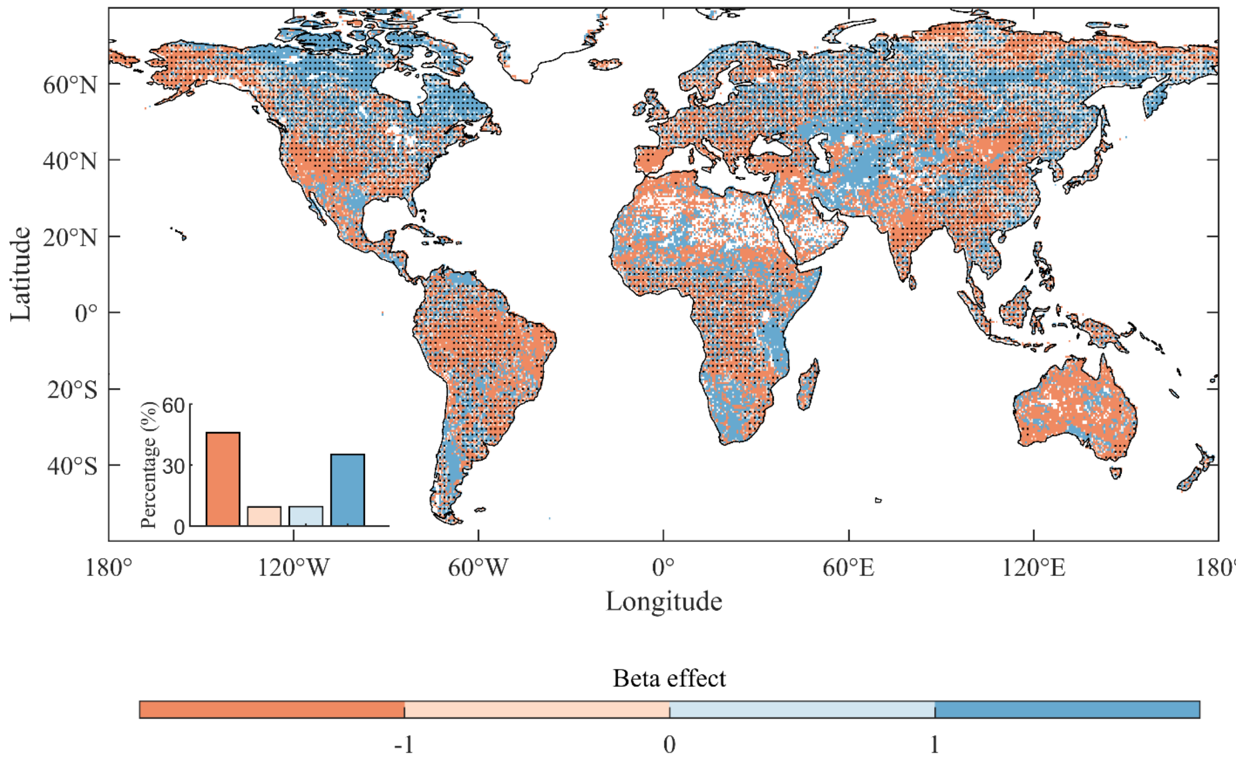

Figure 5. Global distribution of β-factor values under RCP6.0. The β-factor is calculated using the decadal mean CO_2-caused NBP values (difference between RCP-CO_2 and RCP-Control) during 2080-2089 and 2090-2099 and the corresponding atmospheric CO_2 concentrations. The stippling pixels indicate that at least 80% of all the 17 ensemble members have the same sign for the β-factor value. When the β-factor value is less than 1, NBP tends to saturate, and *vice versa*.

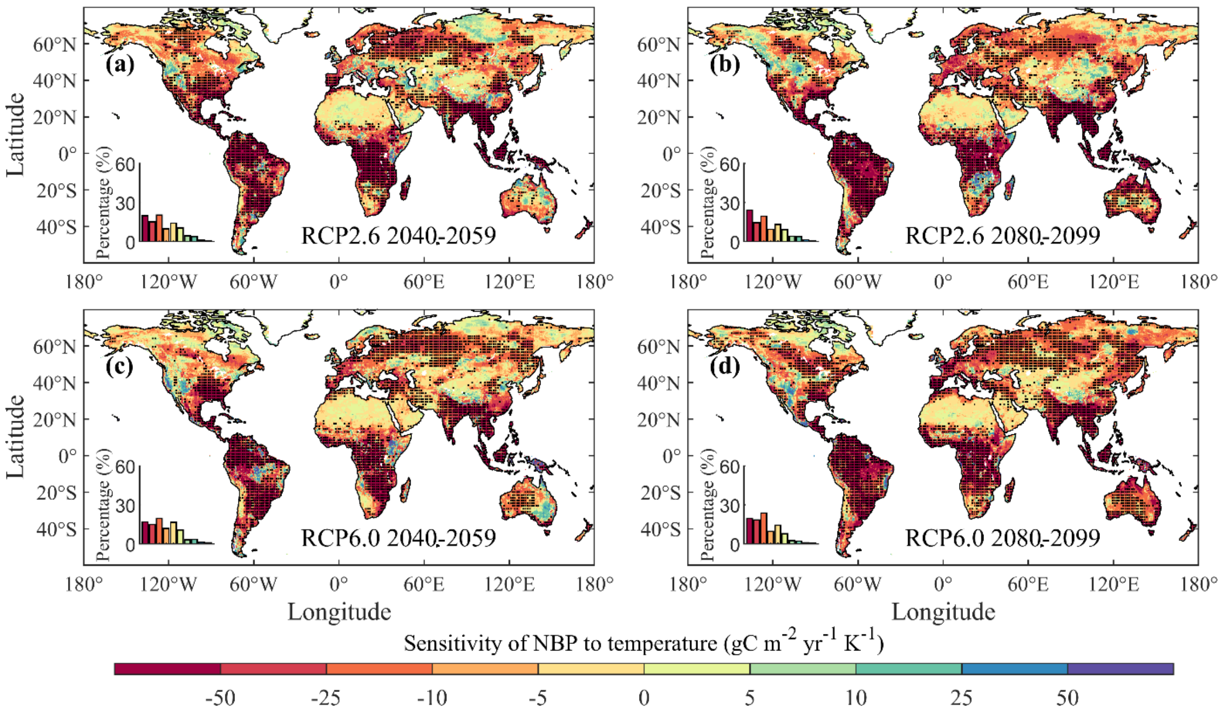

Figure 6. Spatial patterns of the sensitivities of NBP to temperature under RCP2.6 (a, b) and 6.0 (c, d) during 2040-2059 (a, c) and 2080-2099 (b, d), respectively. The insets show histograms of all pixel values. The stippling pixels indicate that at least 80% of all the 17 ensemble members have the same sign for the sensitivity. The sensitivities are derived using RCP-Control experiments.

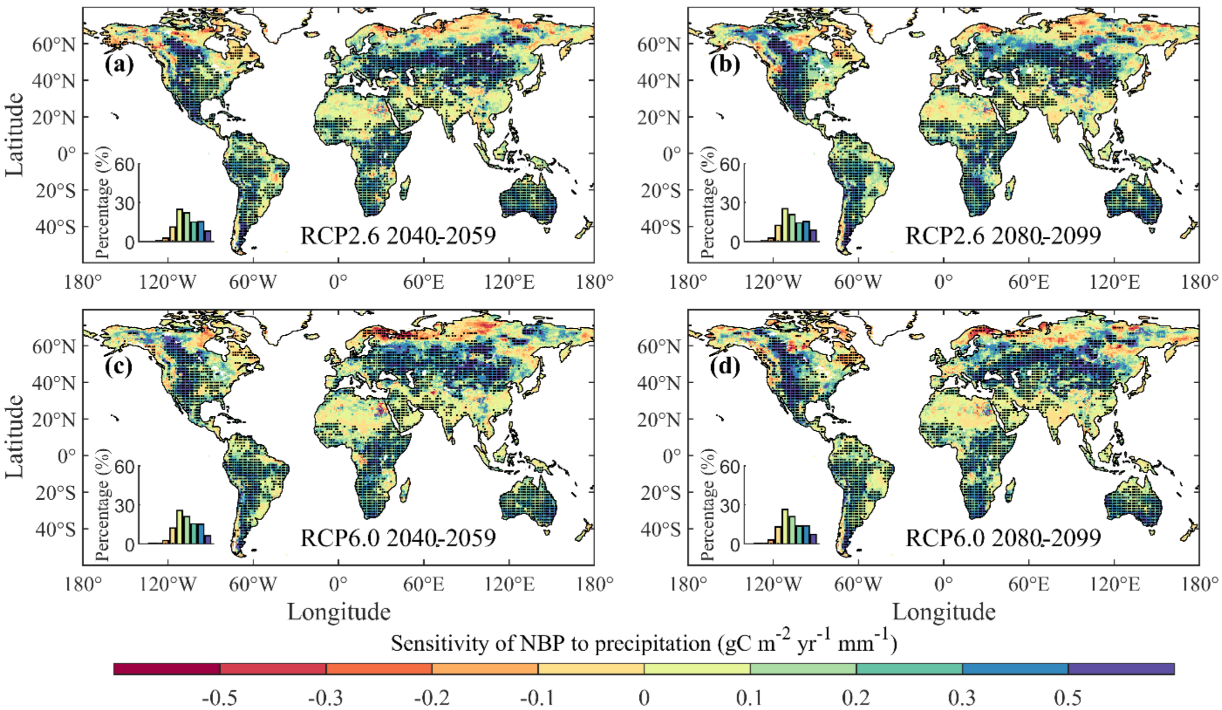

Figure 7. Spatial patterns of the sensitivities of NBP to precipitation under RCP2.6 (a, b) and 6.0 (c, d) during 2040-2059 (a, c) and 2080-2099 (b, d), respectively. The insets show histograms of all pixel values. The stippling pixels indicate that at least 80% of the 17 ensemble members have the same sign for the sensitivity. The sensitivities are derived using RCP-Control experiments.

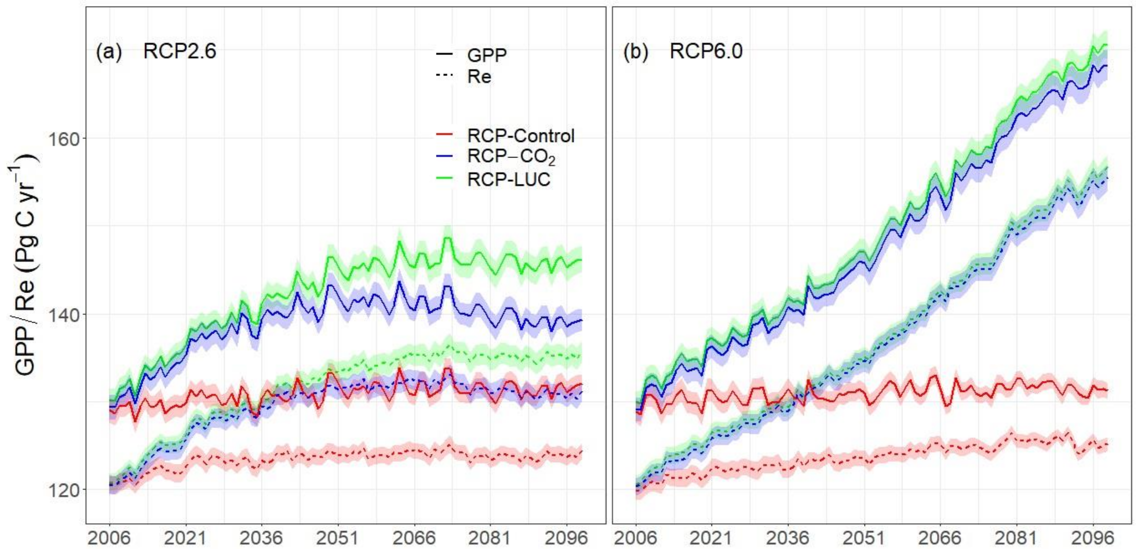

Figure 8. Ensemble mean temporal dynamics of global GPP (solid) and Re (dashed) simulated by different experiments under RCP2.6 (a) and RCP6.0 (b). The shaded areas indicate standard deviations of ensemble mean values. For display, the standard deviations are scaled by a factor of 0.1.

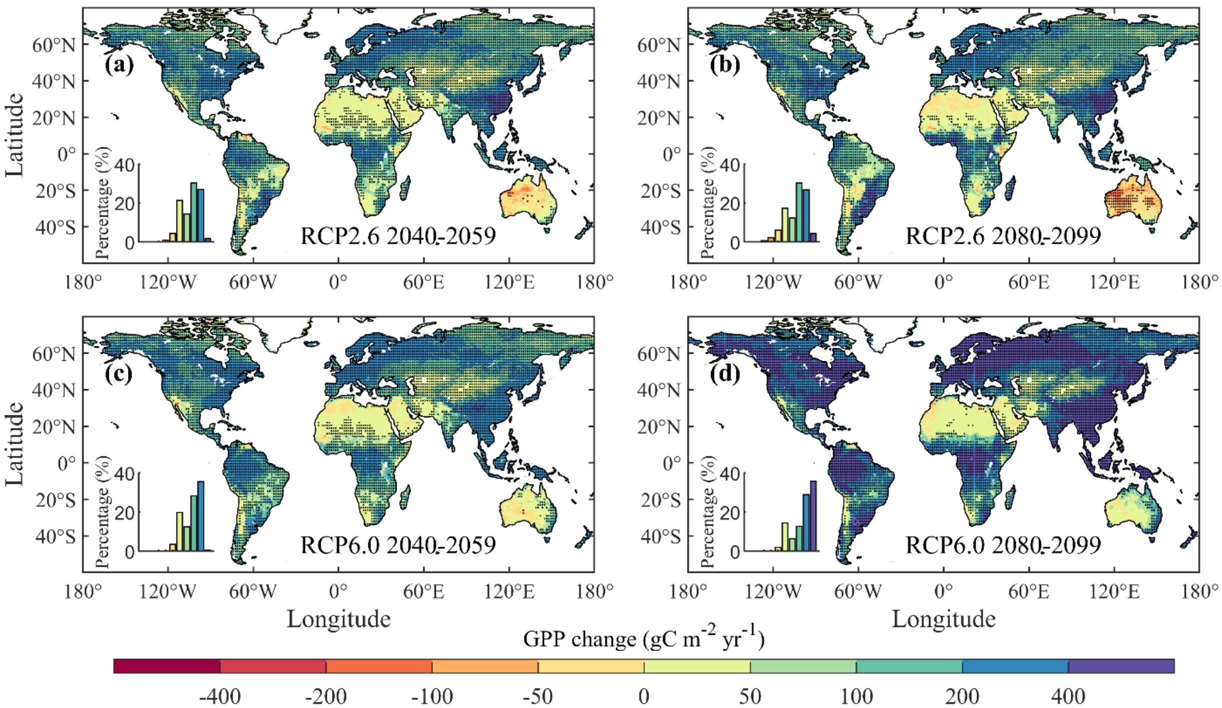

Figure 9. Spatial patterns of GPP changes calculated as the difference between the mean annual GPP during 2040-2059 (a, c) or 2080-2099 (b, d) in the RCP-LUC experiments and that during the historical period under RCP2.6 (a, b) and 6.0 (c, d). The insets show histograms of pixel values of GPP changes. The stippling pixels indicate that at least 80% of all the 17 ensemble members have the same sign for the GPP change.

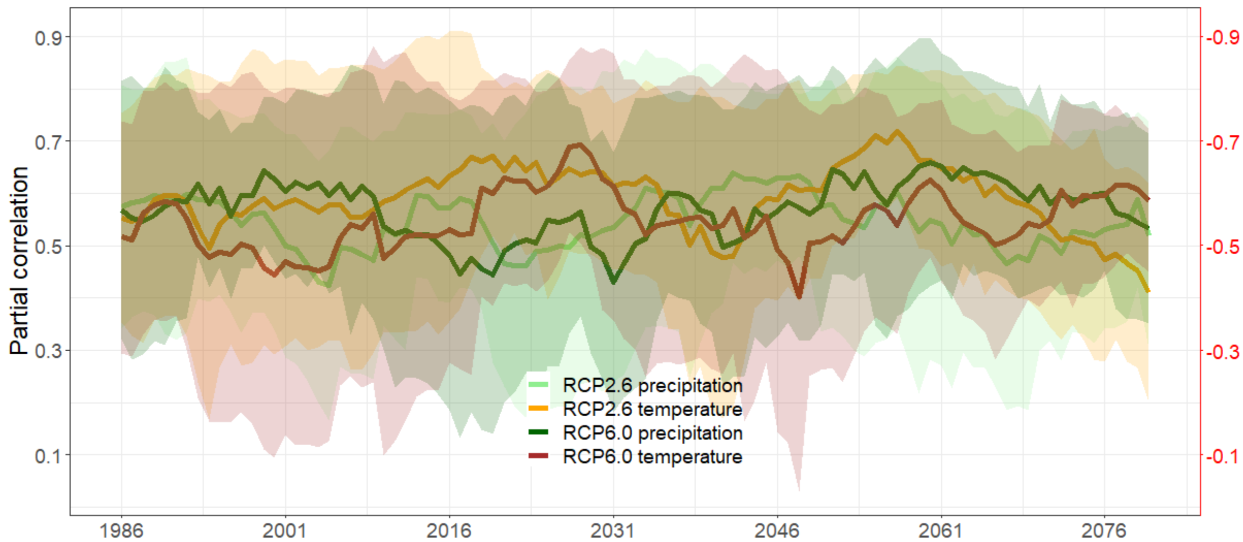

Figure 10. Temporal dynamics of partial correlation between global NBP IAV and temperature IAV or precipitation IAV, calculated by applying a moving 20-year window to the RCP-LUC experiments. Labels of the *x* axis indicate the start year of a moving window. The left *y* axis is for precipitation and the right *y* axis is for temperature. Shaded areas indicate the standard deviation calculated using the 17 ensemble members.

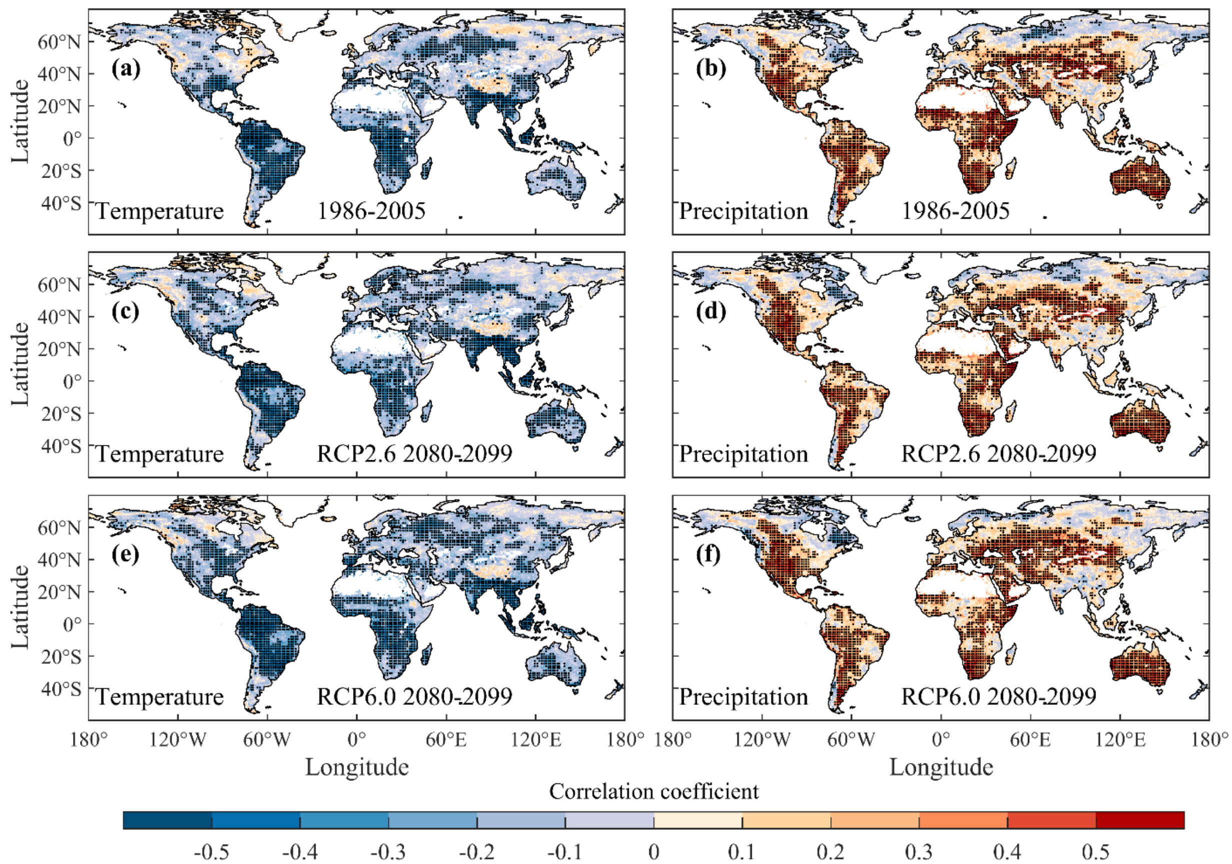

Figure 11. Spatial patterns of partial correlation between NBP IAV and temperature (a, c, e) or precipitation IAV (b, d, f) during the historical period (a, b) or 2080-2099 (c, d, e, f) under RCP2.6 (c, d) and 6.0 (e, f). The stippling pixels indicate that at least 80% of the 17 ensemble members have the same sign for the partial correlation coefficient.